

The Influence of Nickel on Corrosion Behavior of Low Alloy Steel in a Cyclic Wet-dry Condition

Cheng Wen, Yuwan Tian, Gui Wang*, Jiezheng Hu, Peichang Deng

Engineering College, Guangdong Ocean University, Zhanjiang 524088, China

*E-mail: wcheng3jia@163.com

Received: 1 November 2015 / Accepted: 22 February 2016 / Published: 1 April 2016

The marine atmosphere corrosion behavior of a low alloy steel with different nickel contents (0, 0.8, 2, 5 wt%) was studied in the alternate wet-dry conditions (dry/wet conditions). The technique of polarization curves, EIS and SEM were used to study the effect of Ni on the corrosion resistance of four steels, which indicated that the addition of Ni shifted the corrosion potential of the steel in the positive direction and made the corrosion current density lower. The enhancement of the corrosion resistance of steel favored the formation of a homogeneous and compact inner rust layer, and the higher the content of nickel was in the steel, the faster the protective rust layer was generated.

Keywords: corrosion resistance, low alloy steel, cyclic wet-dry condition, nickel

1. INTRODUCTION

Weathering steels always have good corrosion resistance due to the addition of a small amount of alloying elements, such as Cu, P, Cr and so on, and they are widely used in construction industry and auto industry. However, when the atmospheric environment contains excessive chloride ions, the corrosion resistance of conventional weathering steel is not significantly improved [1]. Thus, advanced weathering steels with better corrosion resistance are being developed for use in harsh marine-atmosphere environments.

To obtain steel with better corrosion resistance, Ni has received increasing attention for low alloy steel when used in high atmospheric salinity. There are many studies on the effect of nickel, most of which are mainly confined to fixed nickel contents or the synergistic effects of nickel and other alloying elements, which indicated that the excellent corrosion resistance of weathering steel was mainly attributed to the protective rust layer formed on its surface [2-5]. Many studies have shown that the compact rust layer and good corrosion resistance of nickel-containing steel could be obtained owing to the generation of Fe_2NiO_4 spinel double oxide [6-9]. In a series of reports about advanced

weathering steel containing 3 wt.% nickel, Kimura et al. observed that the formation of Fe_2NiO_4 in the early stage of corrosion provided nucleation sites for nano $\text{Fe}(\text{O},\text{OH})_6$ so that a fine and dense rust would form [10-11]. M. Morcillo [12] noted that it was not as justified to use weathering steel in an indoor environment because the corrosion resistance was almost the same as that of carbon steel. However, weathering steel had an obvious advantage when used in a marine atmosphere due to the formation of protective rust layers, but it was limited to non-marine atmospheres with relatively low corrosivity.

To make better use of steels in a marine atmospheric environment, in this study, we took a low alloy steel as the research object by adding different contents of nickel element to investigate its influence on corrosion performance of steel, which was exposed to the simulated marine atmospheric environment. On the one hand, it is imperative to better understand the corrosion behavior of steel and the role of Ni in more corrosive environment. On the other hand, the paper aims at guiding the composition design of coastal coating-free weathering steel.

2. EXPERIMENTAL PROCEDURES

Carbon steel (Q235) and low alloy steel (0.8Ni, 2Ni and 5Ni with 0.8 wt.%, 2 wt.% and 5 wt.% Ni, respectively) were prepared in this study to investigate the effect of nickel content on the atmospheric corrosion behavior. The content of other alloy elements, such as Cu and Mn, was almost similar in all the steels.

The immersion corrosion test was conducted on the basis of criterion TB/T2375-93 of the Ministry of Railways. In consideration of the deposition of chloride ions and to better simulating the real marine atmospheric environment, a 1.0 wt% NaCl and 0.01 mol/L NaHSO_3 solution was selected as the corrosive electrolyte. The testing samples were cut into 3 mm × 25 mm × 30 mm. Subsequently, four sets of steel samples were exposed to alternate conditions of 12 min immersion in the electrolyte and 48 min drying at 45 ± 2 °C, 60-80% RH. Each cycle was an hour. Samples were taken out after 72, 144, 240 and 360 cycles(hours), respectively. They were then derusted by immersion in a descaling liquid, which consisted of 50 ml hydrochloric acid, 50 ml distilled water and 0.35 g hexamethylenetetramine, for approximately 5-10 min. Subsequently, the sample surfaces were rinsed with deionized water, dried by an air blower, and then weighed to calculate the corrosion mass loss.

Steel samples were ground with SiC sandpapers of 240, 400, 800, 1500 grit in turn and then polished with a polishing paste of 1.5 grain size. Subsequently, they were eroded in 4% nitric acid alcohol solution for the microstructure observation with a QUANTA 250 scanning electron microscope. Electrochemical experiments, performed on a 2273 advanced electrochemical system from Princeton Applied Research were carried out in a 1.0 wt% NaCl and 0.01 mol/L NaHSO_3 solution at 25 ± 1 °C. The electrochemical cell consisted of a saturated calomel reference electrode (SCE), a large Pt mesh that served as the counter electrode and a work electrode with a 10 mm × 10 mm surface area that was ground with 2000 grit SiC sandpaper. The characteristics of the cross section and surface morphology of the steel samples were observed by a digital camera and QUANTA 250 scanning electron microscope after being polished. The EIS experiments were conducted over a

frequency range from 10^4 Hz to 10^{-3} Hz using a 10^{-3} V sinusoidal potential modulation close to the open circuit potential, and the scanning speed was 0.5 mv/s.

3. RESULTS AND DISCUSSION

3.1. Microstructural characterization

No significant microstructural differences were observed between the crosswise and lengthwise sections of the different steels. Fig. 1 shows the representative micrographs of carbon steel and low alloy steel. Compared with Q235, which consisted of ferrite and pearlite with a volume ratio 65 to 35, the microstructure of 0.8Ni and 2Ni had ferrite-granular bainite-lath bainite due to the addition of nickel.

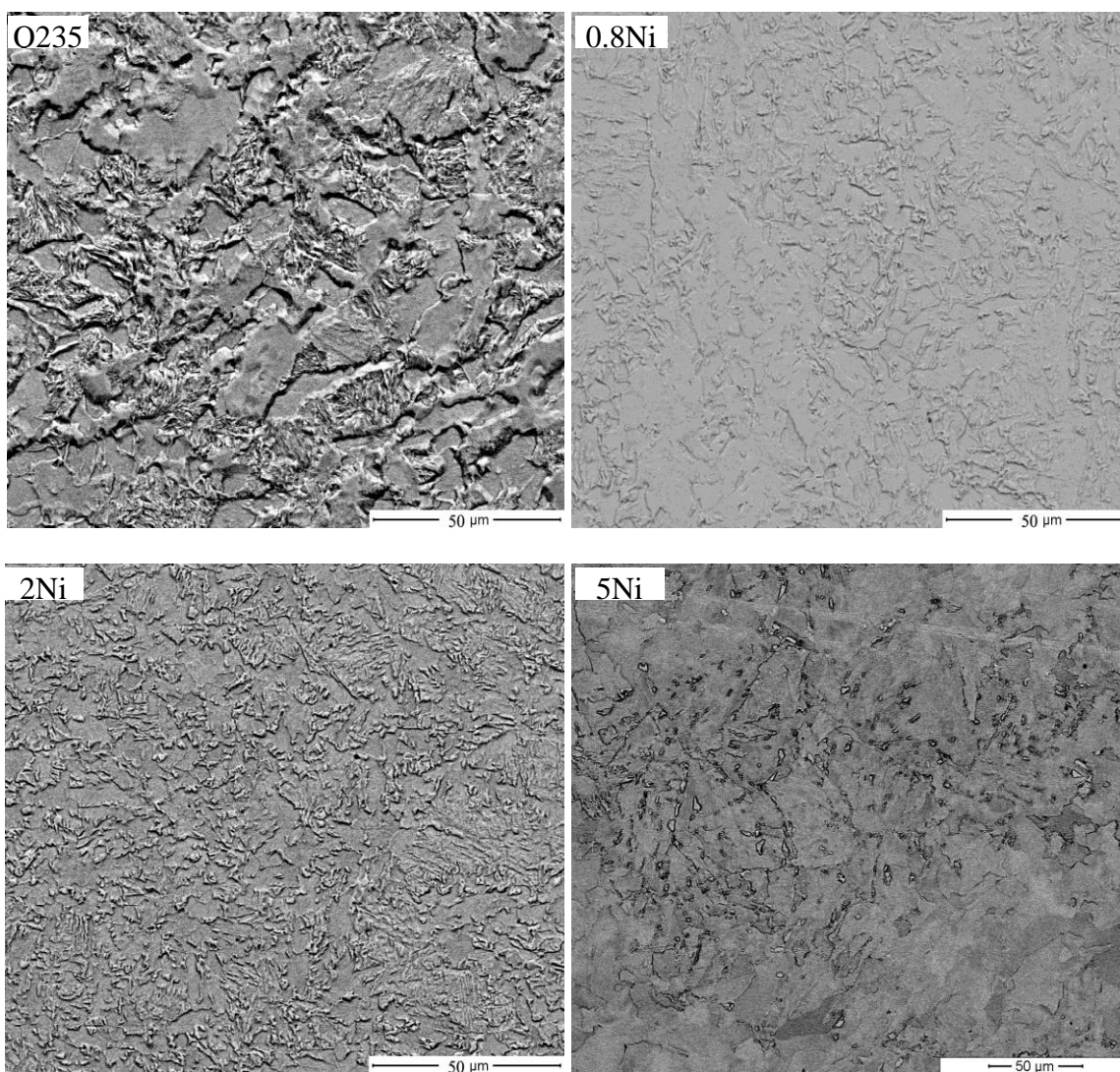


Figure 1. Microstructure of the experimental steels

The microstructure of 5Ni mainly consisted of massive granular bainite, and it also showed the presence of martensite. This is because the alloying element Ni modifies the steel phase transformation diagrams, transformations that have occurred, increasing the hardenability by lowering the critical cooling rate. Moreover, the microstructure was refined with the increase of nickel element, leading to an increase of the grain boundary area and a redistribution of elements, which could influence the corrosion process and the microstructure of steel indirectly [13]. According to the research of Wang et al [14], the effect of the grain size on the atmospheric corrosion resistance of steel can be both a help and a hindrance, which would reflect the indirect effect of nickel contents on the corrosion resistance in this study.

3.2. Electrochemical experiments

The polarization curves and EIS results of carbon steel and low alloy steel measured in the mixed NaHSO₃ and NaCl solution at 25 °C are shown in Fig. 2 and Fig. 3, respectively. The data of the polarization curves and the AC impedance were fitted by ZsimpWin software. The equivalent electric circuit was R(C(R(CR))), where R_s represents the electrolyte resistance, R_c the charge transfer resistance, R_t the rust resistance, C₁ the capacitance of the rust layer, and C₂ the capacitance of the double electric layer, as seen in Fig. 4.

The change of the corrosion potential and current density due to the Ni addition was very remarkable as shown in Fig. 2 and table 1. For the Q235 sample, the corrosion current density is 8.24 μA/cm². Compared with that of carbon steel, the corrosion current density decreased from 6.12 μA/cm² to 3.80 μA/cm² with the addition of Ni, and the corrosion potential of nickel-containing steel tended to be more positive, indicating that with the increase of nickel content, the corrosion rate became lower. However, the difference in the corrosion potential of 2Ni and 5Ni was reduced compared with that of 0.8Ni and 2Ni, and the current density had a similar trend, indicating that the corrosion resistance of low alloy steel was not improved linearly with the addition of nickel element contents.

As shown in Fig. 3, the EIS of the low alloy steels had a similar evolution. The Nyquist curve had two semi-circles, in which a capacitive reactance in the high frequency region was formed from an interfacial electron exchange. The change of the low frequency capacitive reactance indicates that the diffusion process was hindered due to the formation of the protective rust layer on the steel surface. The Nyquist curve of Q235 has only one semi-circle with a smaller diameter, showing that, compared with Q235, nickel-containing steel achieved better corrosion resistance by promoting the formation of protective corrosion products on the steel surface.

It can also be seen from Fig. 3 and table 1 that the charge transfer resistance R_c and rust resistance R_t of the low alloy steel increase with the gradual increase of nickel content. The increase of R_c meant that the corrosion dissolution reaction of the metal substrate was difficult to carry out, but the inhibition effect was mainly because of the formation of the protective rust layer. Therefore, the results indicate that the higher the nickel content was, the more easily the protective rust layer formed. R_t is usually used to evaluate the corrosion resistance of the rust layer directly. From table 1, the R_t value of 0.8Ni was 390, which was significantly higher than that of Q235. Thence, it comes to the conclusion

that the rust layer can effectively prevent the further corrosion of low alloy steel and it had good barrier function, which is in good consistency with the dense structure of the rust layer. According to all the above results, we can know that the corrosion reaction was suppressed by the nickel addition in a certain way.

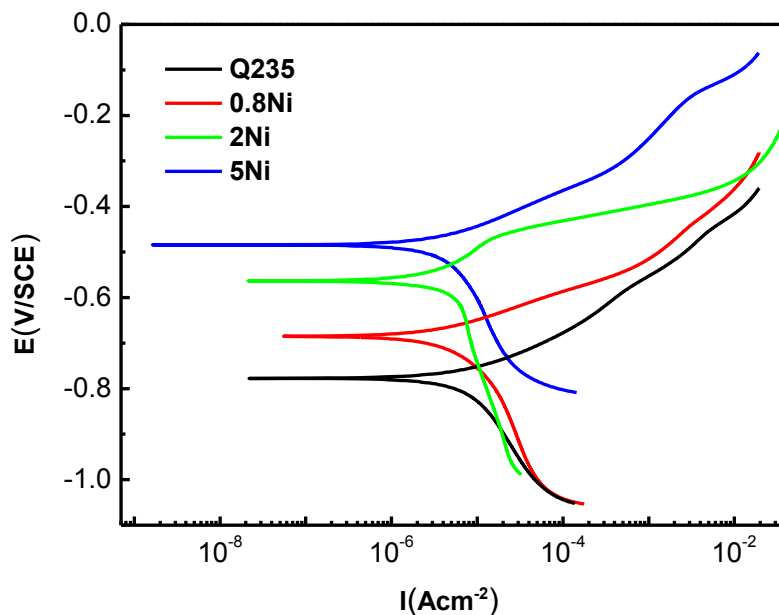


Figure 2. Polarization curves of four steels in 1.0 wt% NaCl and 0.01 mol/L NaHSO₃ before the wet-dry cyclic test

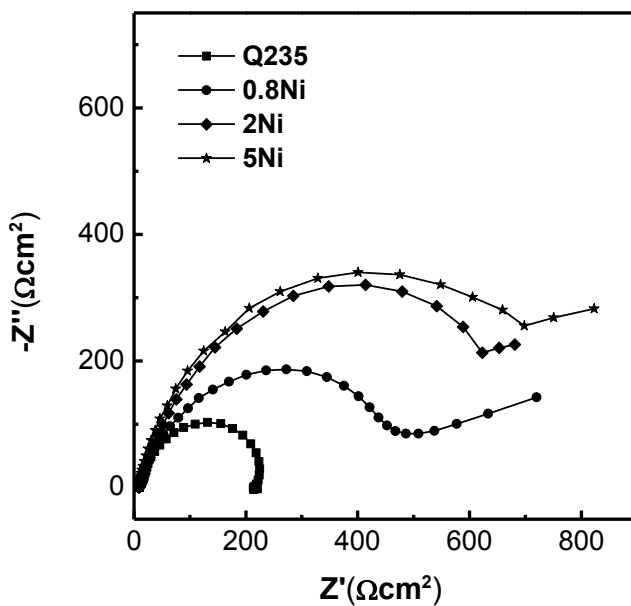


Figure 3. EIS results of four steels in 1.0 wt% NaCl and 0.01 mol/L NaHSO₃ before the wet-dry cyclic test

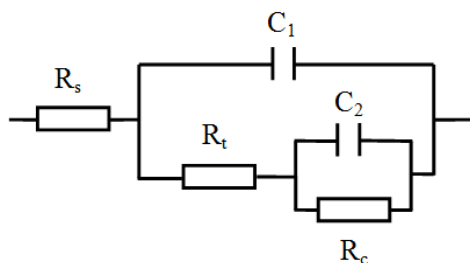


Figure 4. Equivalent circuit used for fitting the EIS results of steel

Table 1. The fitted values of the electrochemical parameters (polarization curves and impedance).

steel	Q235	0.8Ni	2Ni	5Ni
Corrosion potential (mV)	-777	-684	-564	-483
Corrosion current density (μAcm^{-2})	8.24	6.12	5.13	3.80
Tafel slope (β_a) (mV/decade)	99.9	57.9	61.6	79.9
Tafel slope (β_c) (mV/decade)	272.2	236.9	874.4	296.3
R_t (Ωcm^2)	205	390	559	675
R_c (Ωcm^2)	0	262	450	561

3.3. Corrosion mass loss (rate and corrosion kinetic curve)

To eliminate the impact of the density of different steels, the thickness loss was used to assess the corrosion situation. The loss can be obtained by the equation $Tl=m/(\rho \cdot S)$, where m is the mass loss, ρ the density, and S the surface areas of samples. Thus, the corrosion rate was obtained on the basis of thickness loss divided by corrosion cycles (hours). Fig. 5 and Fig. 6 show the corrosion rate and thickness loss of carbon steel and low alloy steel in the simulated marine-atmospheric condition. It can be seen that the corrosion resistance of nickel-containing steel was better than that of carbon steel at every corrosion cycle.

Ch. Thee et al studied the corrosion of a weathering steel under an electrolyte film in a cyclic wet-dry condition and noted that the corrosion rate increases occurred mainly during the drying process because of the increasing concentration of chloride ions, thus enhancing the oxygen diffusion through the thinning electrolyte film [15-16]. In this study, during the first 144 cycles, the corrosion rates of four steels showed little fluctuation, and their thickness loss curves changed with a similar trend. In this stage, the protective rust layer had not yet formed; corrosion was mainly affected by oxygen diffusion and the concentration of chloride ions. However, in the following process after 144 cycles, the corrosion rate of the nickel-containing steel decreased greatly, while for Q235, it basically remained unchanged at a higher value of $0.38 \mu\text{m/h}$. Accordingly, the corrosion could be divided into an initial stage and a later stage by 144 cycles for low alloy steel. The thickness loss value in the initial stage showed that the corrosion resistance was improved with the increase of nickel content, but the effect was negligible. In the later stage, the corrosion rate decreased significantly, which indicated that the protective rust layer as a barrier for oxygen diffusion and chloride ion immersion was generated, and the corrosion resistance increased with the addition of nickel content.

As the cycle proceeded, the rust layer of low alloy steel grew thick with a better protective ability, so the corrosion rate began to decrease greatly. At the 360th cycle, the addition of only 0.8wt.% nickel presented an approximately 2 times lower corrosion loss than that experienced in carbon steel.

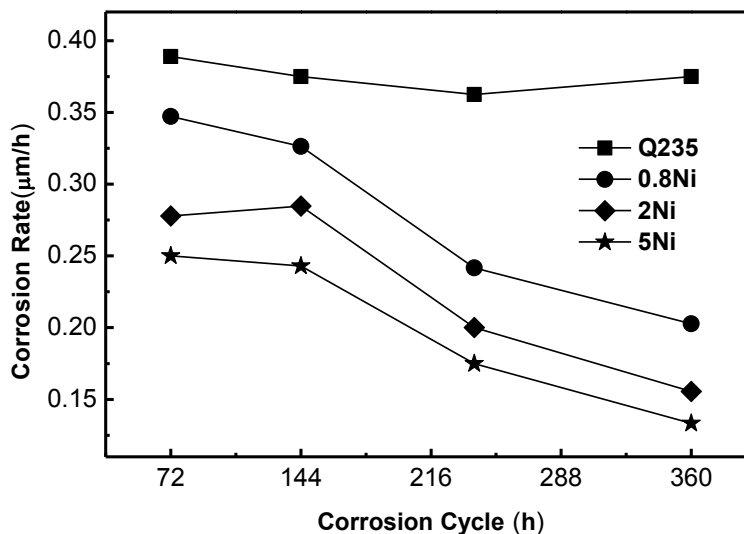


Figure 5. Corrosion rate results of carbon steel and low alloy steel

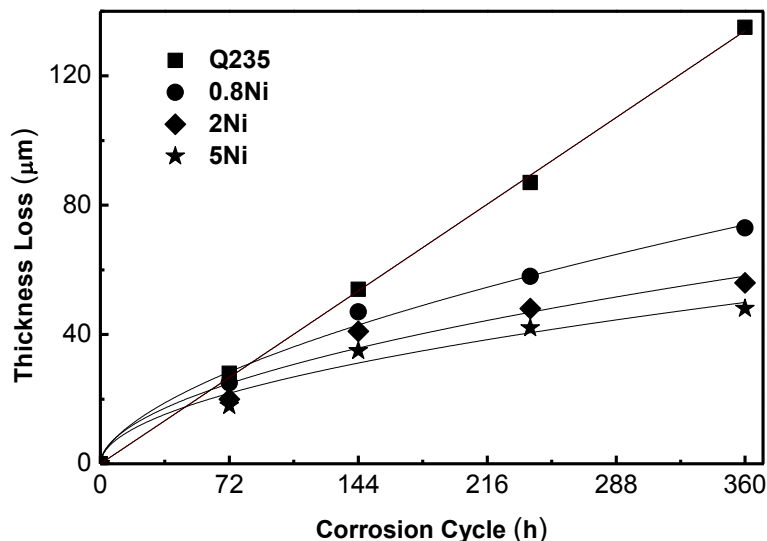


Figure 6. Thickness loss results of carbon steel and low alloy steel

Table 2. Fitted values of corrosion kinetic curves

steel	Q235	0.8Ni	2Ni	5Ni
A	0.368	2.245	2.593	2.416
n	1.002	0.594	0.528	0.515

The variation of thickness loss with corrosion time can be fitted by equation 1, which (also called the bilogarithmic law) is widely used to predict the atmospheric corrosion behavior of metallic materials.

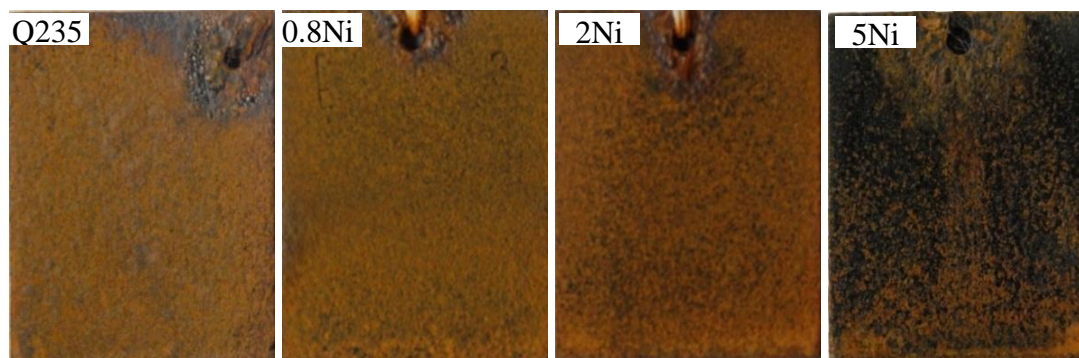
$$\log D = \log A + n \log t \quad (1)$$

where D is the thickness loss (mm), t is the exposure time (years), and A and n are constants. n was used as an indicator for the physico-chemical behavior of the corrosion layer and hence for its interactions with the atmospheric environment. The fitting coefficient values of A and n for different steels are shown in table 2. It can be seen that the n value of Q235 was 1.002, indicating that its corrosion thickness loss increases substantially and almost linearly with the immersion time; that is, the corrosion resistance of the rust layer formed on Q235 maintains a lower value. Referring to the nickel-containing steel, the values of n are all less than 0.6, indicative of corrosion deceleration process caused by the rust layer. According to the research of Dean and Benarie et al [17-18], the exponential law with n close to 0.5, is an ideal diffusion-controlled mechanism when the corrosion products remain on the metal surface, just like what occurs in this investigation, which is consistent with the analysis result of the corrosion rate above. Additionally, the n values changed not very significantly with the increase of nickel content. Thus, nickel addition can affect the property of rust layer and improve the corrosion resistance of low alloy steel, and the nickel addition of 2 wt% seems to be more cost-effective for the design of coating-free weathering steel.

3.4. Corrosion macromorphology

Fig. 7 shows the macromorphology of the rust layer on the four steels. No remarkable morphological changes were found on the rust layers of Q235 in all stages of testing. The loose, porous property and poor adhesion lead to the layered exfoliation of the rust layer, after which the metal substrate was subject to further corrosion, and the corrosion forms included pitting corrosion and general corrosion.

The rusts of the nickel-containing steel were divided into two layers in the later stage of corrosion: a yellow and loose outer layer and a black and compact inner layer. The inner rust layer could reduce the active area of the electrochemical reaction, and prevent the penetration of corrosion ions, such as chloride, effectively.



(a)

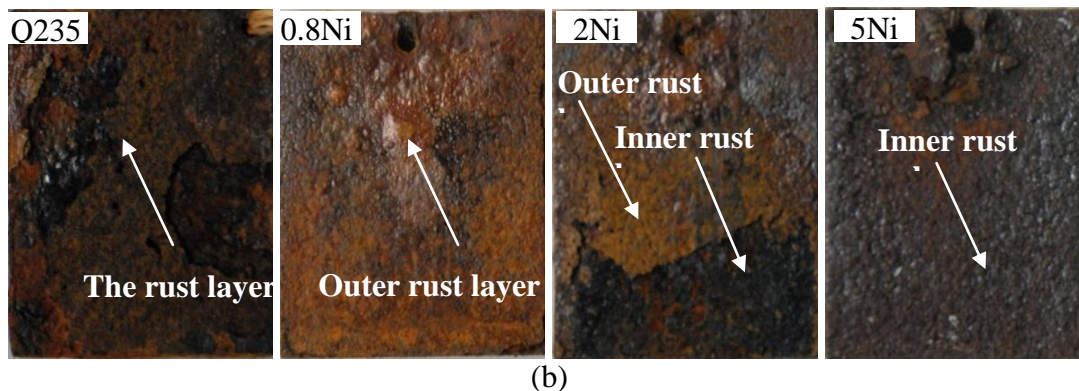


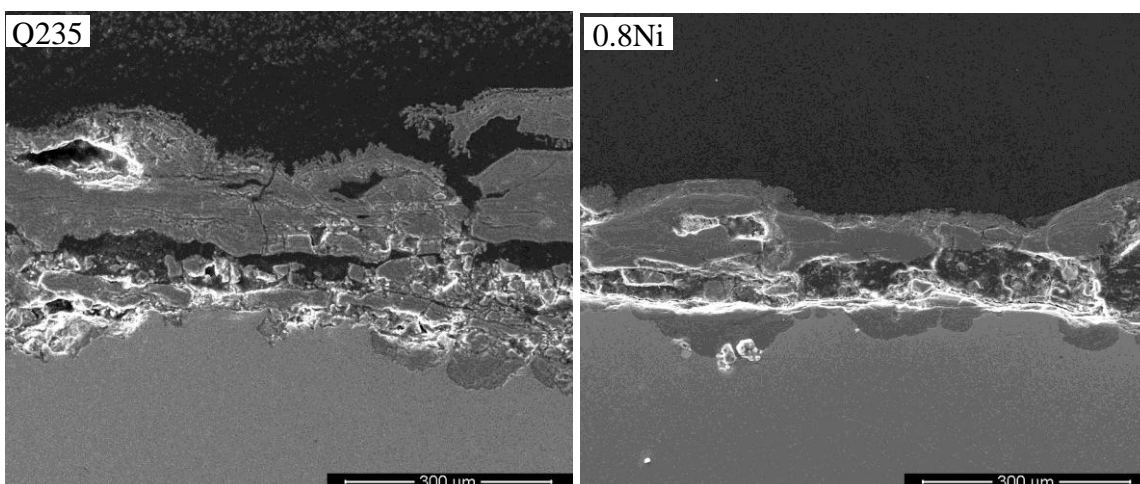
Figure 7. Macromorphology of carbon steel and low alloy steel. (a)72 h; (b)360 h

Furthermore, at the 360th cycle, the rust of 0.8Ni began to form layers, and the outer layer was not yet shed, the outer rust layer of 2Ni was partially shed, while all the outer rust layer of 5Ni was shed, indicating that the higher the nickel content is, the earlier the protective rust forms.

3.5. Corrosion micromorphology

Fig. 8 shows the micromorphology of the cross section of the rust layer on carbon steel and low alloy steel. In all corrosion stages, the rust formed on carbon steel was only one layer that was rougher and more porous than that on the nickel-containing steel surface. The more porous structure of the rust layer led to a less effective barrier against the ingress of precipitation and chloride pollutants and a higher corrosion rate, and the results coincide with the corrosion kinetics curves very well. The poor adhesion and crack-richness of the rust layer led to bubbling, flaking and mass loss.

In addition, the rust layer formed on carbon steel thickened with time, which can improve the corrosion resistance correspondingly, and a greater effect was that the rust layer accelerated corrosion by increasing the wetting time due to corrosive ion retention.



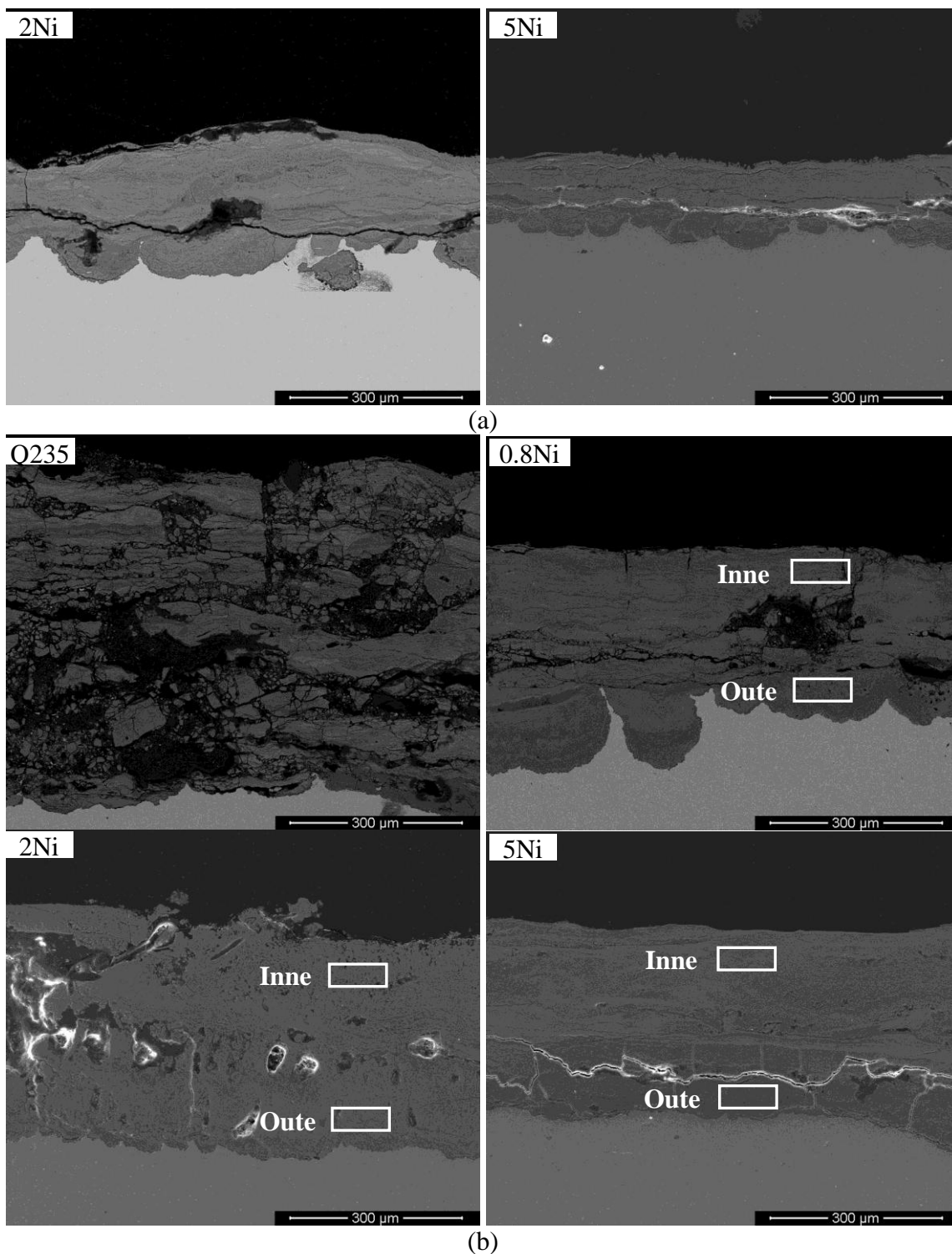


Figure 8. Micromorphology of carbon steel and low alloy steel. (a)72 h; (b)360 h

The rust layer of the nickel-containing steel were composed of outer and inner rust layer. In the literature, it is common to read that the protective nature of rust is associated with its stratification into two sublayers on the steel surface: a adherent and compact inner layer, which accounts for the largest proportion of the sttel’s anticorrosive behavior; and a less adherent and porous outer layer [19-21]. As shown in Fig. 7 and Fig. 8, with the extension of the corrosion cycle, the dense and uniform inner rust

layer was formed, and it was almost crack-free, especially for 2Ni and 5Ni steels, which is considered to be the main mechanism of the better corrosion resistance of nickel containing steel. With the increase of nickel content, the compactness and adhesion of the rust layers became better.

3.6. EDS analysis (Ion-selective property)

Table 3 shows the element content distribution of the inner and outer rust layers after 360 cycles of corrosion in terms of EDS technique.

Kamimura and Alcántara et al [22-23] found that when the deposition amount of chlorine ions reached a certain value, the process of corrosion reaction and the anode and cathode sites would be influenced, thus, the protective ability of the rust layer would be destroyed and the corrosion rate would increase. As seen in table 3, the nickel element was rich especially in the inner rust layer, and the Na^+ content was higher in the outer layer, while the Cl^- content was higher in the inner layer for 0.8Ni steel. In this case, it was easy for Cl^- to penetrate the rust layer to erode the metal substrate, and PH value decreased due to Na^+ hydrolysis which accelerated the anodic dissolution of the metal surface. When the nickel content was higher than 2 wt.%, the opposite distribution resulted, which confirmed the effect of nickel on the ion-selective property. This is mainly because that Ni could replace easily some low-valued atom in the rust layer, thereby forming a cation exchange field [24-25]. It can be inferred that Ni influenced the ion distribution of the rust layer and caused the low alloy steel to exhibit a cation ion-selective property to improve the corrosion resistance. The results are consistent with the variation of corrosion potential as shown in Fig. 5.

Table 3. Distribution of elements in the rust layer (wt.%)

Steel	Rust layer	Ni	Na	Cl
0.8Ni	Outer	0.73	0.35	0.31
	Inner	1.18	0.23	1.24
2Ni	Outer	1.49	0.41	1.43
	Inner	2.65	0.81	0.52
5Ni	Outer	3.53	0.47	0.62
	Inner	3.92	0.91	0.32

4. CONCLUSION

The corrosion behaviors of low alloy steels in a simulated marine atmospheric environment were investigated in this paper. The conclusions summarized from this study are as follows:

(1) Compared with Q235 steel, the rust layer of low alloy steel stratified in the later corrosion stage, and the inner layer closely adhered to the substrate was continuous and compact, which can effectively prevent the penetration of chloride ions and improve the corrosion resistance, as seen from the higher corrosion potential and the lower current density due to the addition of nickel element. The

higher the nickel content was, the earlier the rust stratified.

(2) The atmospheric corrosion behavior of four steels followed the equation $\log D = \log A + n \log t$, in which the n value was 1.002 for Q235 and approximately 0.5 for low alloy steel, attributed to the nickel addition, indicating that the low alloy steel would have a better corrosion resistance when used in high salinity.

(3) The distribution of ions in the rust layer changed when the nickel content of steel was higher than 2 wt.%, so further corrosion would be inhibited, which was important to guiding the composition design of steel to improve corrosion resistance in the coastal environment.

ACKNOWLEDGEMENT

The authors gratefully acknowledge financial support from Program of Accelerated corrosion tests and the accumulation of corrosion data in the harsh marine environment. This work was also supported by the Program of Research on accelerated corrosion experiments and correlation in harsh marine-atmosphere environment (GDOU2014050244) and the Program of accelerated corrosion test technique and protection research in the marine environment.

References

1. F. Corvo, J. Minotas, J. Delgado, C. Arroyave, *Corros. Sci.*, 47(2005) 883-892.
2. Hiroki Tamura, *Corros. Sci.*, 50 (2008) 1872-1883.
3. D.D.N. Singh, Shyamjeet Yadav, Jayant K. Saha, *Corros. Sci.*, 50 (2008) 93-110.
4. J.G. Castana, C.A. Botero, A.H. Restrepo, E.A. Agudelo, E. Correa, F. Echeverria, *Corros. Sci.*, 50 (2010) 216-223.
5. J.H. Wang, F.I. Wei, Y.S. Chang, H.C. Shih, *Mate. Chem. and Phys.*, 47(1997)1-8.
6. Nishimura T, Kodama T, *Corros. Sci.*, 45 (2003)1073-1084.
7. Toshiyasu Nishimura, Hideki Katayama, Kazuhiko Noda, Toshiaki Kodama, *Corros. Sci.*, 42(2000)1611-1621.
8. I. Diaz, H. Cano, D. de la Fuente, B. Chico, J.M. Vega, M. Morcillo, *Corros. Sci.*, 76 (2013)348-360.
9. T. Murata, *Weathering Steel*, Uhlig's Corrosion Handbook, John Wiley and Sons, Inc. New York(2000).
10. M. Kimura, T. Suzuki, G. Shigesato, H. Kihira, K. Tanabe, *Nippon Steel Tech. Report*, 87(2003)17-20.
11. M. Kimura, H. Kihira, N. Ohta, M. Hashimoto, T. Senuma, *Corros. Sci.*, 47(2005)2499-2059.
12. M. Morcillo, B. Chico, I. Díaz, H. Cano, D. de la Fuente, *Corros. Sci.*, 77(2013)6-24.
13. X P Chen, X D Wang, S M Jiang, *J. Mater. Prot.*, 38(2005)14-17.
14. B Wang, Q Y Liu, X D Wang, *Acta. Metall. Sin.*, 48(2012)601-606.
15. Ch. Thee, Long Hao, Junhua Dong, *Corros. Sci.*, 78 (2014) 130-137.
16. A Nishikata, Q J Zhu, E Tada, *Corros. Sci.*, 87 (2014) 80-88.
17. S.W. Dean, D. Knotkova, J.K. Kreislova, ISOCORRAG, ASTM series 71, *West Conshohocken*, 2010.
18. M. Benarie, F.L. Lipfert, *Atmos. Envir.*, 20 (1986) 1947-1958.
19. H. Okada, Y. Hosoi, H. Naito, *Corros.*, 26(1970) 429-430.
20. H. Okada, Y. Hosoi, H. Naito, *Trans. ASM.*, 62(1969) 278-281.
21. Q.C. Zhang, J.S. Wu, J.J. Wang, *Mater. Chem. Phys.*, 77(2003) 603-608.
22. T. Kamimura, K. Kashima, K. Sugae, *Corros. Sci.*, 62 (2012) 34-41.

23. J. Alcántara, B. Chico, I. Díaz, et al, *Corros. Sci.*, 97 (2015) 74-88.
24. Q C Zhang, J J Wang, J S Wu, *Acta. Metall. Sin.*, 2(2001)193-196.
25. Kimura M, Kihira H, Ishi Y, et al, 13th Asian - Pacific Corrosion Control Conference. *Osaka University, Japan*, November, 2003.

© 2016 The Authors. Published by ESG (www.electrochemsci.org). This article is an open access article distributed under the terms and conditions of the Creative Commons Attribution license (<http://creativecommons.org/licenses/by/4.0/>).